2009-12

# Synthesis of (Ca,Nd)Ti'O IND.3' powders by complex polymerization, Rietveld refinement and optical properties

Spectrochimica Acta A,Amsterdam : Elsevier,v. 74, n. 5, p. 1050-1059, Dec. 2009
http://www.producao.usp.br/handle/BDPI/49447

Spectrochimica Acta Part A 74 (2009) 1050–1059

Contents lists available at ScienceDirect

Spectrochimica Acta Part A: Molecular and Biomolecular Spectroscopy

journal homepage: www.elsevier.com/locate/saa

# Synthesis of (Ca,Nd)$TiO_3$ powders by complex polymerization, Rietveld refinement and optical properties

V.S. Marques[a], L.S. Cavalcante[b,*], J.C. Sczancoski[b], E.C. Paris[b], J.M.C. Teixeira[a], J.A. Varela[c], F.S. De Vicente[d], M.R. Joya[b], P.S. Pizani[b], M. Siu Li[d], M.R.M.C. Santos[a], E. Longo[c]

[a] CCN-Química, Universidade Federal do Piauí, 64049-550, Teresina, PI, Brazil
[b] Departamento de Química/Física-UFSCar, P.O. Box 676, 13565-905, São Paulo, Brazil
[c] Instituto de Química-UNESP, P.O. Box 355, 14801-907, Araraquara, SP, Brazil
[d] Instituto de Física de São Carlos, USP, P.O. Box 369, 13560-970, São Carlos, SP, Brazil

ARTICLE INFO

*Article history:*
Received 19 February 2009
Received in revised form 25 August 2009
Accepted 26 August 2009

*Keywords:*
$(Ca_{0.99}Nd_{0.01})TiO_3$
Rietveld refinement
*f–f* transitions
Photoluminescence

ABSTRACT

Neodymium calcium titanate, $(Ca_{0.99}Nd_{0.01})TiO_3$ powders were synthesized by the complex polymerization method and heat treated at different temperatures for 2 h under air atmosphere. The structural evolution of these powders as a function of heat treatment temperature was analyzed by X-ray diffraction (XRD) and micro-Raman (MR) spectroscopy. The optical properties were investigated by Ultraviolet–visible (UV–vis) absorption spectroscopy and Photoluminescence (PL) measurements. XRD patterns, Rietveld refinement and MR spectra indicated that the powders heated treated at 750 °C for 2 h present an orthorhombic structure without secondary phases. UV–vis measurements suggested the presence of intermediary energy in disordered $(Ca_{0.99}Nd_{0.01})TiO_3$ powders. Broad and narrow bands were observed in the PL spectra of these powders when excited with 350 nm wavelength. The broad bands were associated to the structural defects and/or *p–d* electronic transitions while, the narrow bands were ascribed to *f–f* transitions arising from $Nd^{3+}$ ions.



## 1. Introduction

In the last years, several studies have been reported in the literature on the structural phase transitions of calcium titanate ($CaTiO_3$) as a function of temperature and pressure [1–5]. In particular, this perovskite has a wide potential for applications in resonators and filters due to its high-dielectric constant and low-dielectric loss at high frequencies [6–14]. When doped with rare earth trivalent ions ($La^{3+}$, $Sm^{3+}$ or $Nd^{3+}$), the dielectric properties of $CaTiO_3$ can be modified as consequence of the formation of $Ca^{2+}$ vacancies into the lattice [13,14]. On the other hand, this material is considered an incipient ferroelectric or quantum paraelectric at low temperatures. In this case, small perturbations (electric fields, elastic strains and impurities) can destroy the structural stability and induce a ferroelectric phase [15]. Lemanov et al. [16] reported a phase transition from incipient to normal ferroelectric state in $Ca_{1-x}Pb_xTiO_3$ solid solutions with Pb content up to $x = 0.3$.

Currently, this perovskite has been employed for different technological purposes. For example, the formation of a $CaTiO_3$ interface layer on the hydroxyapatite-coated Ti substrates is able to increase the bond strength of this system as well as decrease the progression of hydroxyapatite dissolution in acidic environment, which is produced by osteoclastic resorption in the human body [17–19]. Also, $CaTiO_3$ phase has contributed to the fast precipitation and deposition of silicon-substituted hydroxyapatite coatings on titanium substrates through the biomimetic method [17]. In the electrochemical area, Wang et al. [20] reported that $CaTiO_3$-coated Ti electrodes modified with a thin hydrophobic layer are more corrosion resistance than the $TiO_2$-coated Ti electrodes. In addition, $Zr^{4+}$-doped $CaTiO_3$ powders (from 5 mol% to 7 mol%) [21] and CoO/$CaTiO_3$ catalysts [22] present a high efficiency in the water conversion process into hydrogen. In terms of photoluminescence properties, the $CaTiO_3$ has been mainly investigated when doped with $Pr^{3+}$, $Eu^{3+}$ and $Sm^{3+}$ ions [23–32]. The use of these rare earth lanthanides into the matrix of this ceramic material results in the formation of red phosphors, except for the $Sm^{3+}$, which it has been employed as an optical probe in order to estimate the degree of structural order. However, the literature does not report studies on the optical properties of $Nd^{3+}$-doped $CaTiO_3$.

Different synthesis methods have been employed for the formation of this perovskite, mainly including: solid-state reaction or mechanochemical [33–37], molten salts [38–40], self-propagating high temperature [41–43], topochemical microcrystal conversion [44] and ultrasonic mist combustion/pyrolysis processes [45]. However, these methods present some drawbacks, such as: formation of secondary phases, contamination by impuri-

* Corresponding author. Tel.: +55 16 3361 5215; fax: +55 16 3351 8214.
*E-mail address:* laeciosc@bol.com.br (L.S. Cavalcante).

1386-1425/$ – see front matter © 2009 Elsevier B.V. All rights reserved.
doi:10.1016/j.saa.2009.08.049

ties, high heat treatment temperatures, long processing times and nonuniform particle size distribution. In order to overcome these problems, the wet chemical methods can be significantly more effective, for example: sol–gel [46–50], inorganic salt sol–gel [51], hydrolysis of metal alkoxides [52], co-precipitation [53,44], polymeric precursor [54–56], hydrothermal method [57–59] and hydrothermal–electrochemical [60]. Also, these synthesis methods are able to improve the dielectrical, structural and morphological properties of $CaTiO_3$ ceramics [61–64]. In particular, the complex polymerization method (CPM) has become a versatile chemical route in which pure compounds are formed at low heat treatment temperatures with short processing times. In this chemical route, the chelation process of the metal cations by a hydroxycarboxylic acid reduces the phase segregation and favor a homogeneous cation distribution at molecular scale into the polymeric resin [65].

Therefore, in this work, $(Ca_{0.99}Nd_{0.01})TiO_3$ powders were synthesized for the first time by the complex polymerization method (CPM) and heat treated at different temperatures for 2 h under air atmosphere. These powders were structurally characterized by X-ray diffraction, Rietveld refinement and micro-Raman (MR) spectroscopy. The optical properties were analyzed by ultraviolet–visible (UV–vis) absorption spectroscopy and photoluminescence (PL) measurements.

## 2. Experimental details

### 2.1. Synthesis of $(Ca_{0.99}Nd_{0.01})TiO_3$ powders

The $(Ca_{0.99}Nd_{0.01})TiO_3$ powders were synthesized by the CPM. In this synthesis method, calcium carbonate $CaCO_3$ (99% Aldrich), titanium (IV) isopropoxide $[Ti(OC_3H_7)_4]$ (98% Acros Organics), ethylene glycol $C_2H_6O_2$ (99.5% Synth), citric acid anhydrous $C_6H_8O_7$ (99.5% Synth) and neodymium oxide $Nd_2O_3$ (99.9% Aldrich) were used as raw materials. Initially, $C_6H_8O_7$ was dissolved in deionized water heated at 75 °C under constant stirring. Afterwards, $[Ti(OC_3H_7)_4]$ was quickly added into this citric acid aqueous solution to avoid hydrolysis reaction between alkoxide and air environment. This chemical mixture after heated at 90 °C under constant stirring for several hours resulted in the formation of a clear and homogenous titanium citrate solution. The gravimetric procedure was performed to estimate the stoichiometric value correspondent to the mass (g) of titanium oxide contained into the citrate. In the sequence, a stoichiometric quantity of $CaCO_3$ was dissolved into this titanium citrate solution. A neodymium solution was prepared through the dissolution of $Nd_2O_3$ in nitric acid and then, it was mixed with the calcium–titanium citrate solution. After solution homogenization, $C_2H_6O_2$ was added in order to promote the citrate polymerization by the polyesterification reaction. The citric acid/ethylene glycol mass ratio was fixed at 60:40 wt%. The resulting solution was heated at 120 °C under constant stirring to eliminate water, consequently forming a polymeric resin. This polymeric resin was then placed in a conventional furnace and heat treated at 300 °C for 4 h to promote the pulverization and decomposition of organic compounds arising from $C_6H_8O_7$ and $C_2H_6O_2$. Finally, the obtained precursors were heat treated at different temperatures in the range from 300 °C to 750 °C for 2 h under air atmosphere.

### 2.2. Characterizations of $(Ca_{0.99}Nd_{0.01})TiO_3$ powders

The $(Ca_{0.99}Nd_{0.01})TiO_3$ powders were characterized by X-ray powder diffraction (XRD) using a DMax/2500PC diffractometer (Rigaku, Japan). XRD patterns were obtained using Cu-K$\alpha$ radiation in the $2\theta$ range from 5° to 75°, while the Rietveld routine was performed in the $2\theta$ range from 10° to 110°, using a scanning rate

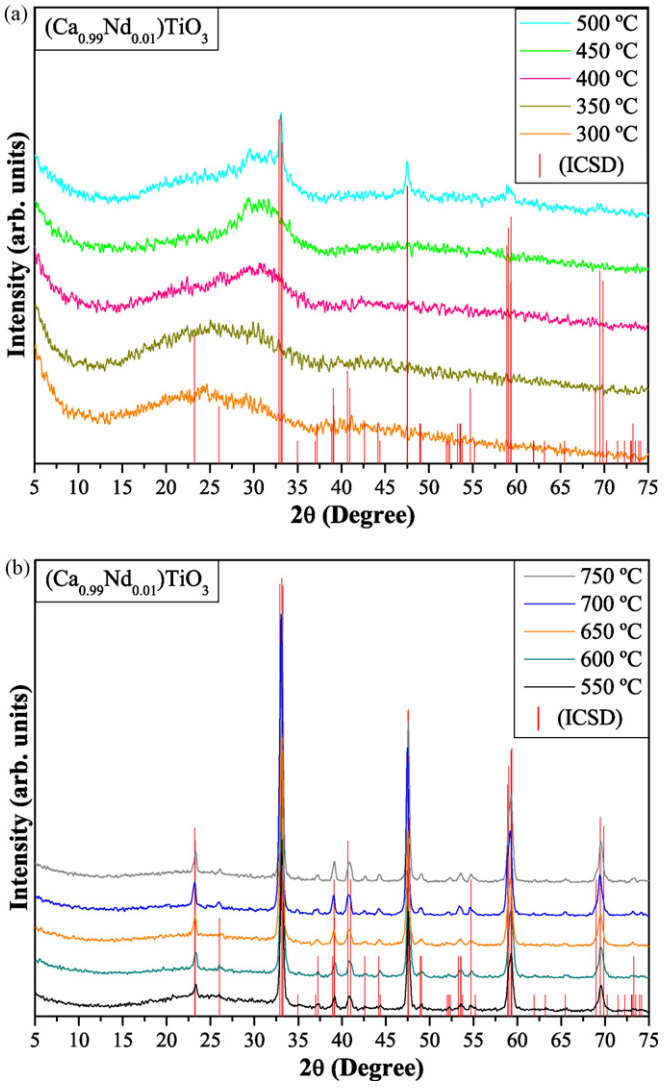


**Fig. 1.** XRD patterns of $(Ca_{0.99}Nd_{0.01})TiO_3$ powders heat treated from: (a) 300 °C to 500 °C and (b) 550 °C to 750 °C at different temperatures for 2 h under air atmosphere.

of 0.2°/s. MR measurements were performed using a T64000 spectrometer (Jobin-Yvon, France) triple monochromator coupled to a CCD detector. The spectra were obtained using an argon ion laser of 514.5 nm, keeping its maximum output power at 9 mW. A 100 μm lens was used to prevent sample overheating. UV–vis spectra were taken using a Cary 5G (Varian, USA) equipment in total reflection mode. PL measurements were performed through a Monospec 27 monochromator (Thermal Jarrel Ash, USA) coupled to a R446 photomultiplier (Hamamatsu, Japan). A krypton ion laser of 350 nm (Coherent Innova 90 K, USA) was used as excitation source, keeping its maximum output power at 200 mW. UV–vis and PL spectra were taken three times for each sample in order to ensure the reliability of the results. All measurements were performed at room temperature.

## 3. Results and discussion

### 3.1. X-ray diffraction and Rietveld refinement analyses

Fig. 1(a and b) shows the XRD patterns of $(Ca_{0.99}Nd_{0.01})TiO_3$ powders heat treated at different temperatures for 2 h under air atmosphere.

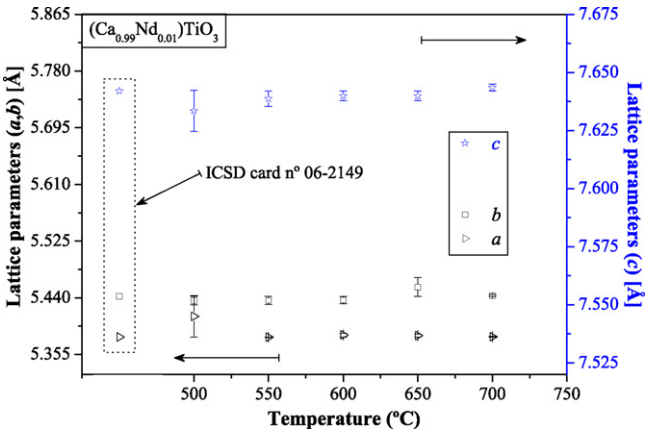


**Fig. 2.** *a*, *b* and *c* lattice parameters of $(Ca_{0.99}Nd_{0.01})TiO_3$ powders as a function of heat treatment temperature.

The presence of diffraction peaks can be used to evaluate the structural order at long-range or periodicity of the material [66]. All powders heat treated from 300 °C to 450 °C do not exhibited diffraction peaks ascribed to $(Ca_{0.99}Nd_{0.01})TiO_3$ phase, evidencing a typical behavior of material in amorphous state or considered as structurally disordered at long-range (Fig. 1a). After heat treatment performed in the range from 550 °C to 750 °C, it was observed a progressive increase in the degree of crystallization of these powders because of the formation of intense and well-defined diffraction peaks (Fig. 1b). In addition, XRD patterns corresponding to the secondary phases were not detected, indicating that the $Nd^{3+}$ ions were incorporated into the $CaTiO_3$ lattice. The diffraction peaks of crystalline $(Ca_{0.99}Nd_{0.01})TiO_3$ powders were indexed to the orthorhombic structure, in agreement with the respective Inorganic Crystal Structure Database (ICSD) card N°. 06-2149 [67].

Fig. 2 shows the lattice parameter values of $(Ca_{0.99}Nd_{0.01})TiO_3$ powders heat treated from 500 °C to 700 °C for 2 h under air atmosphere.

The experimental lattice parameters were calculated using the least square refinement with the UNITCELL-97 program [68]. From the results presented in Fig. 2, it is possible to note that the lattice parameter values of $(Ca_{0.99}Nd_{0.01})TiO_3$ powders presented small deviations from those reported in ICSD card N°. 06-2149 [67] for the pure $CaTiO_3$ phase. Hence, we believe that this behavior can be caused by the differences between the ionic radius of $Ca^{2+}$ (1.14 Å) and $Nd^{3+}$ (1.27 Å). On the basis of this affirmation, possibly the substitution of $Ca^{2+}$ by $Nd^{3+}$ ions is able to induce small anisotropic distortions and/or strains along the $CaTiO_3$ lattice, modifying consequently the *a*, *b* and *c* lattice parameters. Also, these structural defects can be arising from the transformation process from disordered to ordered structure, mainly during the initial stages of heat treatment where the residual organic compounds are gradually eliminated from the matrix. Hence, the influence of these structural defects on the lattice parameters can be minimized with the increase of heat treatment temperature (Fig. 1).

Fig. 3 shows the Rietveld refinement performed on the $(Ca_{0.99}Nd_{0.01})TiO_3$ powder heat treated at 750 °C for 2 h under air atmosphere.

The Rietveld refinement is a method in which the profile intensities obtained from step-scanning measurements of the powders allow to estimate an approximate structural model for the real structure [69]. In our work, the Rietveld refinement was performed through the GSAS program [70]. In the Rietveld analysis, the refined parameters were scale factor, background, shift lattice constants, profile half-width parameters $(u, v, w)$, isotropic thermal parameters, strain anisotropy factor, occupancy, atomic functional positions, bond lengths and bond angles. Firstly, the Rietveld

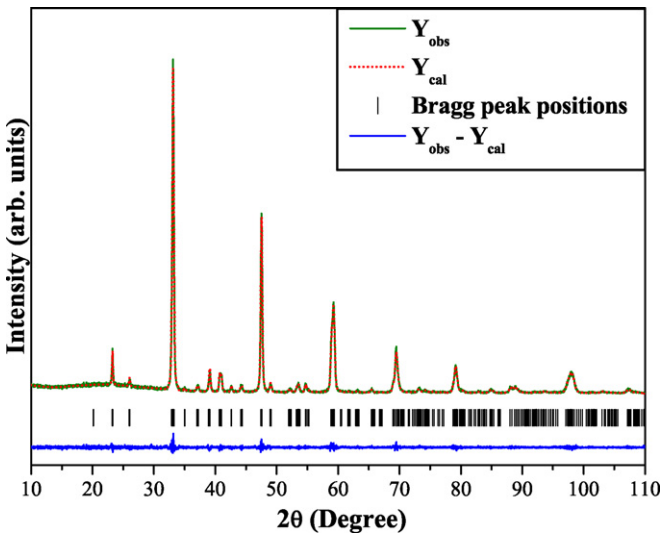


**Fig. 3.** Rietveld refinement of $(Ca_{0.99}Nd_{0.01})TiO_3$ powders heat treated at 750 °C for 2 h under air atmosphere.

refinement was based on the $CaTiO_3$ phase with perovskite-type orthorhombic structure and space group *Pbnm* as indicated in ICSD card N°. 06-2149 [67]. The background was corrected using a Chebyschev polynomial of the first kind. The diffraction peak profiles were better fitted by the Thompson–Cox–Hastings pseudo-Voigt (pV-TCH) function and by the asymmetry function described by Finger et al. [71]. The strain anisotropy was corrected by the phenomenological model described by Stephens [72]. The obtained results from the Rietveld refinement are displayed in Table 1.

In this table, the fitting parameters ($R_p$, $R_{wp}$ and $\chi^2$) indicate a good agreement between the refined and observed XRD patterns for the $(Ca_{0.99}Nd_{0.01})TiO_3$ phase. The refined lattice parameter values ($a = 5.390562$ Å; $b = 5.443374$ Å and $c = 7.649834$ Å) and bond angles ($\alpha = \beta = \gamma = 90°$) confirmed that the $(Ca_{0.99}Nd_{0.01})TiO_3$ phase has an orthorhombic structure. These Rietveld refinement results obtained in this work are in good agreement with those reported in the literature [73–79].

### 3.2. Micro-Raman spectroscopy analyses

Fig. 4(a and b) show the MR spectra of $(Ca_{0.99}Nd_{0.01})TiO_3$ powders heat treated at different temperatures for 2 h under air atmosphere.

The MR spectroscopy is considered a powerful tool in order to estimate the degree of structural order–disorder at short-range of the materials [66]. According to the literature [80–82], there are 24 Raman-active modes for the orthorhombic structure with four molecular units in the primitive cell and space group *Pbnm* ($Z^B = 4$). Hence, its irreducible representation at the Γ point of the Brillouin zone for the lattice vibrations can be described by $\Gamma_{Raman,Pbnm} = 7A_g + 5B_{1g} + 7B_{2g} + 5B_{3g}$.

**Table 1**
Rietveld refinement results and atomic coordinates employed to model the $(Ca_{0.99}Nd_{0.01})TiO_3$ unit cell.

| Atom | Site | *x* | *y* | *z* |
|---|---|---|---|---|
| Calcium | 4c | −0.0049(7) | 0.0343(6) | 0.25 |
| Neodymium | 4c | −0.0049(7) | 0.0343(6) | 0.25 |
| Titanium | 4b | 0.0 | 0.5 | 0.0 |
| Oxygen1 | 4c | 0.0699(3) | 0.4868(2) | 0.25 |
| Oxygen2 | 8d | 0.7096(2) | 0.2911(2) | 0.0366(2) |

$R_{Bragg} = 3.87$, $R_p = 7.39$, $R_{wp} = 10.36$ and $\chi^2 = 1.238$.

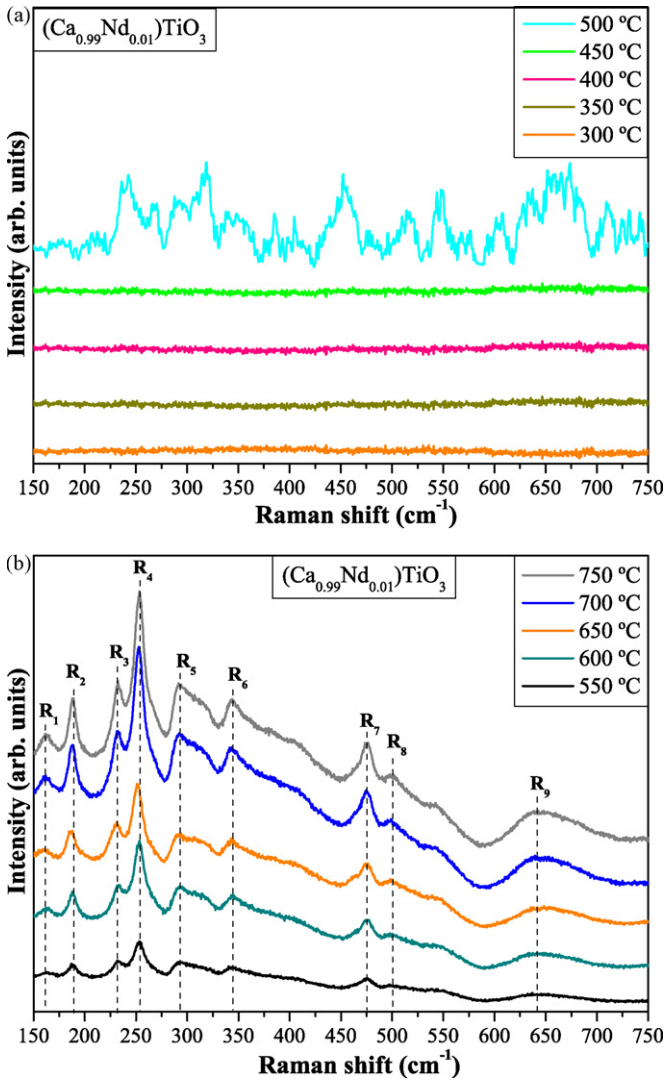


**Fig. 4.** MR spectra of $(Ca_{0.99}Nd_{0.01})TiO_3$ powders heat treated from: (a) 300 °C to 500 °C and (b) 550 °C to 750 °C for 2 h under air atmosphere.

As it can be seen in Fig. 4(a and b), only 9 ($R_1$, $R_2$, $R_3$, $R_4$, $R_5$, $R_6$, $R_7$, $R_8$ and $R_9$) from the 24 Raman-active modes were detected in the MR spectra of $(Ca_{0.99}Nd_{0.01})TiO_3$ powders. Thus, we believe that all bands were not observed in the MR spectra because some can be overlapping with other intense bands or due to the small changes in polarizability [82]. Raman-active modes were not detected for the powders heat treated from 300 °C to 500 °C (Fig. 4(a)). It is an indicative that these powders are disordered at short-range. The presence of well-defined Raman-active modes was verified only for the powders heat treated from 550 °C to 750 °C. Therefore, these temperature conditions are able to increase the structural organization and reduce the structural defects in the lattice. As consequence, this mechanism promotes a stronger interaction between the ions, which mainly arise from the stretching, torsional and bending vibrations of the shorter metal-oxygen bonds, contributing to the observation of the Raman-active modes. Table 2 shows a comparative between the positions of Raman-active modes obtained in this work for the $(Ca_{0.99}Nd_{0.01})TiO_3$ powders with those reported in the literature for the pure $CaTiO_3$ phase [80,83–86].

According to Hirata et al. [84], the $R_1$ band is related to the $CaTiO_3$ lattice mode. Balachandran and Eror [85] reported that the $R_2$, $R_3$, $R_4$, $R_5$ and $R_6$ bands are ascribed to O–Ti–O bending vibration modes or caused by the tilting phenomenon between the $[TiO_6]$–$[TiO_6]$ clusters. The $R_7$ and $R_8$ bands are attributed to the torsional modes, while the $R_9$ band is assigned to the Ti–O symmetric stretching vibration mode [86]. The slight shifts observed on the characteristic positions of Raman modes listed in Table 1, can be related to the degree of crystallization, interaction force between ions, presence of structural defects (oxygen vacancies, distortions and/or strains in the structure) and/or influence of doping ions into the $CaTiO_3$ lattice. The band situated at 641 $cm^{-1}$ ($R_9$) for the $(Ca_{0.99}Nd_{0.01})TiO_3$ powders becomes more defined with the increase of heat treatment temperature. In this case, at high temperatures (from 650 °C to 750 °C) occur stronger interactions between the Ti–O bonds, suggesting an increase in the formation of $[TiO_6]$–$[TiO_6]$ clusters into the structure.

### 3.3. Ultraviolet–visible absorption spectroscopy analyses

Fig. 5(a–f) show the UV–vis absorbance spectra of $(Ca_{0.99}Nd_{0.01})TiO_3$ powders heat treated at different temperatures for 2 h under air atmosphere.

The optical band gap energy ($E_{gap}$) was estimated by the method proposed by Wood and Tauc [87]. According to these authors, the optical band gap is associated with absorbance and photon energy by the following equation:

$$h\nu\alpha \propto (h\nu - E_{gap})^k, \quad (1)$$

where $\alpha$ is the absorbance, $h$ is the Planck constant, $\nu$ is the frequency, $E_{gap}$ is the optical band gap and $k$ is a constant associated to the different types of electronic transitions ($k = 1/2, 2, 3/2$ or 3 for direct allowed, indirect allowed, direct forbidden and indirect forbidden transitions, respectively). According to literature [55,96], the titanates are characterized by an indirect allowed electronic transition and hence, the $k = 2$ value was adopted as standard in Eq. (1). Thus, the $E_{gap}$ values were evaluated extrapolating the linear portion of the curve or tail $[(h\nu\alpha)^{1/k} = 0)]$ in the UV–vis absorbance spectra.

A plausible explanation for the variations observed on the $E_{gap}$ values can be related to the degree of structural order–disorder into the lattice, which is able to change the intermediary energy level distribution within the band gap. For the disordered $(Ca_{0.99}Nd_{0.01})TiO_3$ powders heat treated from 300 °C to 500 °C, the UV–vis absorbance measurements suggest an optical band

**Table 2**
Comparative results between the positions of Raman-active modes obtained in this work for the $(Ca_{0.99}Nd_{0.01})TiO_3$ phase with those reported in the literature for the pure $CaTiO_3$ phase.

| M | T (°C) | t (min) | $R_1$ | $R_2$ | $R_3$ | $R_4$ | $R_5$ | $R_6$ | $R_7$ | $R_8$ | $R_9$ | Ref. |
|---|---|---|---|---|---|---|---|---|---|---|---|---|
| SSR | 1050 | 4320 | 154 | 181 | 225 | 246 | 286 | 335 | 470 | 494 | – | [80] |
| SSR | 1650 | 240 | – | 183 | 227 | 247 | 288 | 339 | 470 | 494 | 641 | [83] |
| SSR | 1250 | 1080 | – | 175 | 224 | 244 | 286 | 336 | 471 | 492 | 677 | [84] |
| LMT | 800 | – | 155 | 180 | 226 | 247 | 286 | 337 | 471 | 495 | – | [85] |
| SSR | 1600 | 2880 | 153 | 178 | 222 | 244 | 281 | 333 | 467 | 490 | – | [86] |
| CP | 750 | 120 | 161 | 188 | 232 | 253 | 291 | 344 | 475 | 501 | 641 | This work |

M, method; T, temperature; t, time; assignments Raman modes ($R_n$): ($cm^{-1}$). Preparation methods: SSR, solid-state reactions; LMT, liquid mix technique; CP, complex polymerization; and Ref., references.

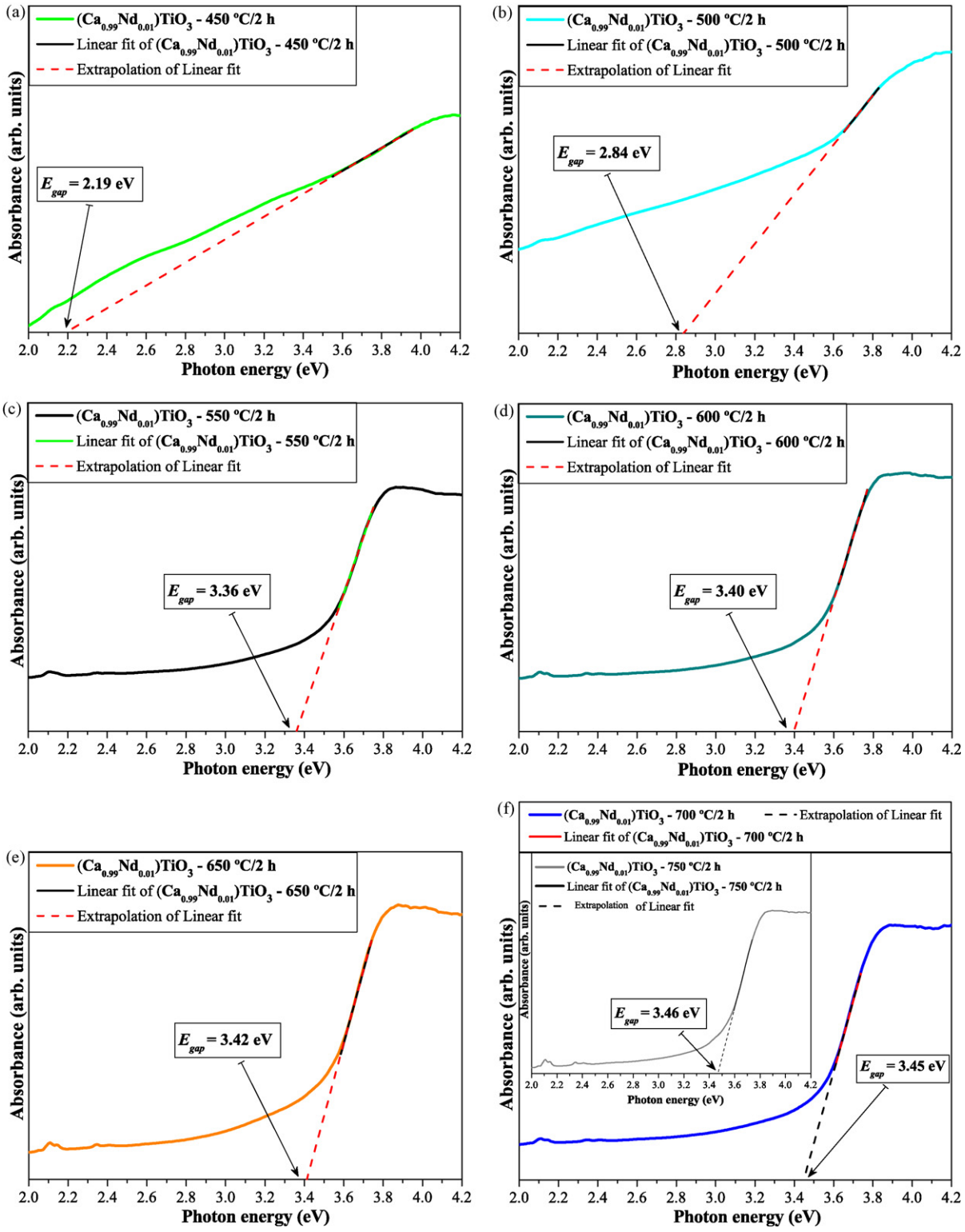


**Fig. 5.** UV–vis absorbance spectra of $(Ca_{0.99}Nd_{0.01})TiO_3$ powders powders heat treated at different temperatures: (a) 450 °C, (b) 500 °C, (c) 550 °C, (d) 600 °C, (e) 650 °C and (f) 700 °C for 2 h under air atmosphere. Inset in Fig. 5(f) shows the UV–vis absorbance spectra of $(Ca_{0.99}Nd_{0.01})TiO_3$ powders heat treated at 750 °C.

gap behavior of materials in amorphous state or with a high degree of structural defects (Fig. 5a and b), while the powders heat treated from 550 °C to 750 °C present a typical absorption spectra of ordered or crystalline materials (Fig. 5c–f). On the basis of these informations, if the structure becomes more ordered with the heat treatment temperature, i.e., when the concentration of structural defects (oxygen vacancies, distortions and/or strains in the lattice) is reduced, the presence of intermediary energy levels (deep and shallow holes) is minimized within the optical band gap of $(Ca_{0.99}Nd_{0.01})TiO_3$ powders and consequently the $E_{gap}$ values increase.

Table 3 shows a comparative between the optical band gap values of $(Ca_{0.99}Nd_{0.01})TiO_3$ powders obtained in this work with those reported in the literature for the $CaTiO_3$ phase [55,89–92]. The $E_{gap}$

**Table 3**
Comparative results between the optical band gap energy of $(Ca_{0.99}Nd_{0.01})TiO_3$ powders obtained in this work with those reported in the literature for the pure $CaTiO_3$ phase.

| Method | Temperature (°C) | Time (min) | Optical band gap (eV) | Ref. |
|---|---|---|---|---|
| PP | 600 | 120 | 3.48 | [55] |
| CPP | 600 | 300 | 3.55 | [88] |
| CSS | 1400 | 720 | 3.30 | [90] |
| HT-C | 497 | – | 3.50 | [91] |
| – | – | – | 3.70 | [92] |
| CP | 450 | 120 | 2.19 | This work |
| CP | 500 | 120 | 2.84 | This work |
| CP | 550 | 120 | 3.36 | This work |
| CP | 600 | 120 | 3.40 | This work |
| CP | 650 | 120 | 3.42 | This work |
| CP | 700 | 120 | 3.45 | This work |
| CP | 750 | 120 | 3.46 | This work |

PP, polymeric precursor; CPP, complex polymer precursor; CSS, conventional solid state; HT-C, hydrothermal-calcination and CPM, complex polymerization; and Ref., reference.

values of $CaTiO_3$ phase were adopted as standard, since for the $(Ca_{0.99}Nd_{0.01})TiO_3$ phase has not been reported in the literature yet.

As it can be seen in this table, the $E_{gap}$ values are mainly dependents of the preparation methods and experimental conditions (heat treatment temperature and processing time). In particular, these key factors can favor or inhibit the formation of structural defects, which are able to control the degree of structural order–disorder of the material and consequently, the number of intermediary energy levels within the band gap. In addition, it is well acceptable that the small percentage of $Nd^{3+}$ ions used as dopant can influence in the $E_{gap}$ of pure $CaTiO_3$ phase.

### 3.4. Schematic representation for the $(Ca_{0.99}Nd_{0.01})TiO_3$ unit cell: symmetric and asymmetric structures

Fig. 6(a and b) shows a schematic representation of two unit cells in order to explain the structural organization process of $(Ca_{0.99}Nd_{0.01})TiO_3$ powders prepared by the complex polymeric method. These unit cells were modeled through the Diamond Crystal and Molecular Structure Visualization (Version 3.1 for Windows) program [93], using the atomic coordinates obtained from the Rietveld refinement (Table 1).

Fig. 6(a) shows a schematic representation of an orthorhombic $(Ca_{0.99}Nd_{0.01})TiO_3$ unit cell with space group *Pbnm* (N° 62). Basically, this crystalline or ordered structure presents the Ti atoms coordinated to six oxygen atoms ($[TiO_6]$–$[TiO_6]$ clusters) in an octahedral configuration. These octahedrons are tilted into this distorted structure, presenting angles between the polyhedrons [Ti–O–Ti] of approximately 157° and 203°, respectively [94]. In principle, the octahedral tilting is associated with the Goldschmidt tolerance factor. Thus, a low value of this factor suggests the presence of available spaces for tilt into the structure [95]. In this perovskite-type structure, the Ca atoms are coordinated to twelve oxygen in a dodecahedral configuration [96], while the Nd atoms are bonded to seven oxygen in a heptahedral configuration [97]. However, these coordinations were not represented in the $(Ca_{0.99}Nd_{0.01})TiO_3$ unit cell in order to favor the visualization of $[TiO_6]$ complex clusters (octahedral configuration).

Fig. 6(b) shows schematic representation of an orthorhombic $(Ca_{0.99}Nd_{0.01})TiO_3$ unit cell with structural order–disorder due to the presence of $[TiO_5]$–$[TiO_6]$ clusters, which is known as asymmetric structure. In this kind of structure, four Ti atoms were displaced along the [001] direction (*z*-axis) in order to represent the $[TiO_5.V_O^z]$ intermediate complex clusters with pyramidal-type configuration, where $V_O^z = V_O^x$, $V_O^{\bullet}$ and $V_O^{\bullet\bullet}$. In the last years, studies performed by means of X-ray absorption near edge structure [98], extended X-ray absorption fine structure (EXAFS) and X-ray photoelectron spectroscopy measurements have revealed the presence of $[TiO_6]$–$[TiO_5]$ clusters into the lattice of different titanates [99–101]. Hanajiri et al. [99] used the EXAFS technique in order to understand the influence of doping ions ($Ce^{3+}$ and $Nd^{3+}$) on the local structure of $CaTiO_3$ powders. According to these authors, the Ti–O distances decreased when the $Nd^{3+}$ content was increased into this perovskite. In an opposite situation, the high concen-

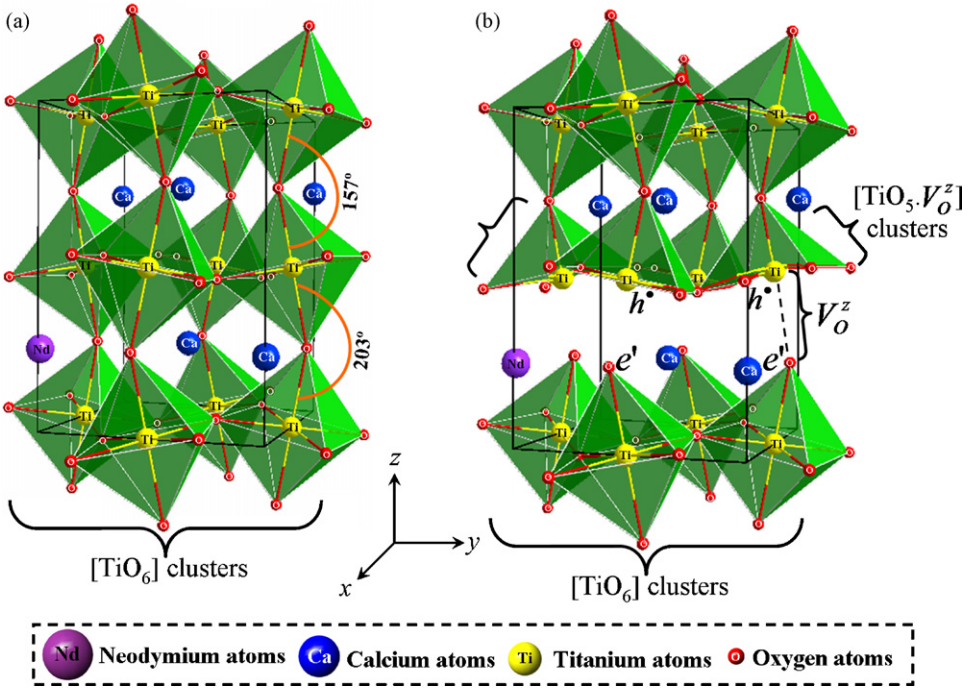


**Fig. 6.** Schematic representation of a (a) model symmetric or ordered $(Ca_{0.99}Nd_{0.01})TiO_3$ unit cell ($[TiO_6]$–$[TiO_6]$ clusters) and a (b) model asymmetric or disordered $(Ca_{0.99}Nd_{0.01})TiO_3$ unit cell ($[TiO_5]$–$[TiO_6]$ clusters).

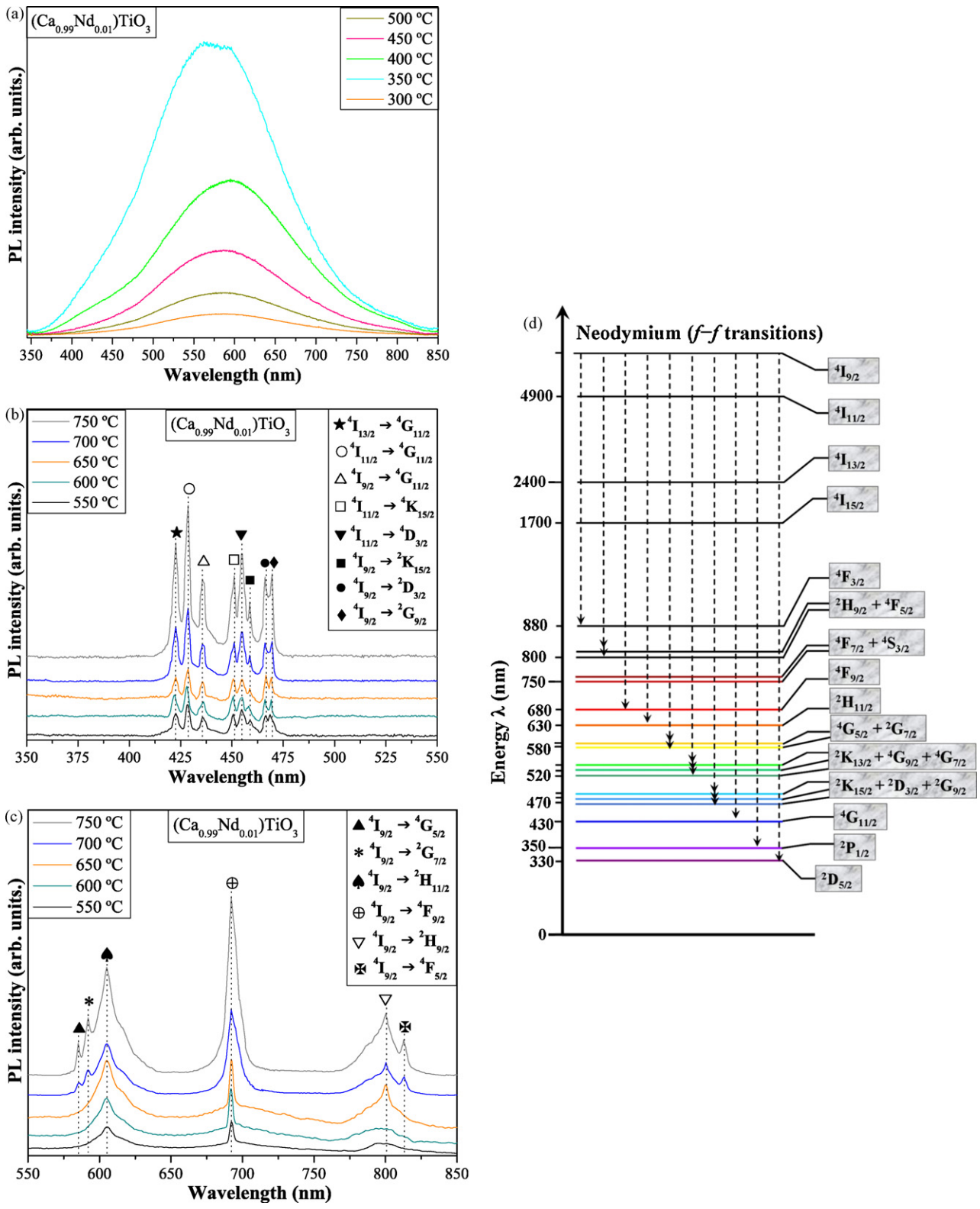


**Fig. 7.** PL spectra of $(Ca_{0.99}Nd_{0.01})TiO_3$ powders heat treated (a) from 300 °C to 500 °C, (b) from 550 °C to 750 °C (in the range from 350 $cm^{-1}$ to 550 $cm^{-1}$), (c) from 550 °C to 750 °C (in the range from 550 $cm^{-1}$ to 850 $cm^{-1}$) under air atmosphere and (d) energy level diagram for the *f–f* electronic transitions arising from $Nd^{3+}$ ions.

tration of $Ce^{3+}$ content into the $CaTiO_3$ powders resulted in an increase between the Ti–O distances. Vance et al. [100] reported that the introduction of dopants ($Gd^{3+}$) into the $CaTiO_3$ structure leads to a charge compensation via reduction from $Ti^{4+}$ to $Ti^{3+}$ specimens.

In the unit cell shown in Fig. 6(b), the structural defects were attributed to the oxygen vacancies, which are able to present three different charge states: (I) neutral ($V_O^x$)—it is able to donate up to two electrons, (II) singly ionized ($V_O^\bullet$)—it donates or capture only one electron and (III) double ionized ($V_O^{\bullet\bullet}$)—it is not able to donate

electrons. In particular, the double ionized charge states ($V_O^{\bullet\bullet}$) are considered the most responsible for the charge transfer in a material with perovskite-type structure, playing an important role in the conduction process. Another important point to be considered is that the replacement of trivalent ions ($Nd^{3+}$) into sites normally occupied by divalent ions ($Ca^{2+}$) leads to a negative charge compensation into the $CaTiO_3$ lattice. This behavior can be described by the following equations:

$$Nd_2O_3 \xrightarrow{CaTiO_3} 2Nd_{Ca}^{\bullet} + V_{Ca}'' + 3O_O^x \quad (2)$$

In this work, the proposed models were based on the supposition of a reduction caused in the number of oxygen vacancies ([$TiO_5$. $V_O^z$ intermediate complex clusters) into the ($Ca_{0.99}Nd_{0.01}$)$TiO_3$ lattice due to the increase of structural organization promoted by the heat treatment temperatures. In order to understand this phenomenon, it was used the Kröger–Vink notation for systems containing the presence of complex clusters [102,103]. Thus, the complex oxygen vancancies ($V_O^x$, $V_O^{\bullet}$ and $V_O^{\bullet\bullet}$) stabilize the lattice defects via charge compensation.

For the network formers:

$$[TiO_6]^x + [TiO_5.V_O^x] \rightarrow [TiO_6]' + [TiO_5.V_O^{\bullet}] \quad (3)$$

$$[TiO_6]^x + [TiO_5.V_O^{\bullet}] \rightarrow [TiO_6]' + [TiO_5.V_O^{\bullet\bullet}] \quad (4)$$

For the network modifiers:

$$[CaO_{12}]^x + [CaO_{11}.V_O^x] \rightarrow [CaO_{12}]' + [CaO_{11}.V_O^{\bullet}] \quad (5)$$

$$[CaO_{12}]^x + [CaO_{11}.V_O^{\bullet}] \rightarrow [CaO_{12}]' + [CaO_{11}.V_O^{\bullet\bullet}] \quad (6)$$

$$[NdO_7]^x + [NdO_6.V_O^x] \rightarrow [NdO_7]' + [NdO_6.V_O^{\bullet}] \quad (7)$$

$$[NdO_7]^x + [NdO_6.V_O^{\bullet}] \rightarrow [NdO_7]' + [NdO_6.V_O^{\bullet\bullet}] \quad (8)$$

In these equations, [$TiO_5$. $V_O^x$], [$CaO_{11}$. $V_O^x$] and [$NdO_6$. $V_O^x$] complex clusters are electron donor species; $[TiO_6]^x$, $[CaO_{12}]^x$ and $[NdO_7]^x$ complex clusters are electron acceptor species; [$TiO_5$. $V_O^{\bullet}$], [$CaO_{12}$. $V_O^{\bullet}$] and [$NdO_6$. $V_O^{\bullet}$] are electron donor–acceptor species. The $[TiO_6]'$, $[CaO_{12}]'$ and $[NdO_7]'$ with [$TiO_5$. $V_O^{\bullet}$], [$CaO_{11}$. $V_O^{\bullet}$] and [$NdO_6$. $V_O^{\bullet}$] complex clusters results in a stabilization of the defects by the charge compensation.

### 3.5. Photoluminescence analyses: emission spectra of ($Ca_{0.99}Nd_{0.01}$)$TiO_3$ powders

Fig. 7(a–c) show the photoluminescence (PL) spectra of ($Ca_{0.99}Nd_{0.01}$)$TiO_3$ powders heat treated at different temperatures for 2 h under air atmosphere. The energy level diagram corresponding to the $Nd^{3+}$ ions is shown in Fig. 7(d).

The powders heat treated from 300 °C to 500 °C exhibited an intense and broad PL emission with a maximum situated at around 566 nm (yellow light emission) (Fig. 7a). We believe that the origin of this phenomenon is caused by a symmetry break into the ($Ca_{0.99}Nd_{0.01}$)$TiO_3$ structure due to the formation of [$TiO_5$. $V_O^z$] intermediate complex clusters ($V_O^z = V_O^x$, $V_O^{\bullet}$ and $V_O^{\bullet\bullet}$) (Fig. 6b). These kinds of clusters, arising from oxygen vacancies, cause the formation of intermediary energy levels within the band gap, which are able to trap electrons. In principle, these energy levels are basically composed of oxygen 2*p* (near the valence band) and titanium 3*d* states (below the conduction band). The electronic transitions between theses states can be classified as charge-transference processes from [$TiO_5$. $V_O^{\bullet}$] to $[TiO_6]'$ and/or [$CaO_{11}$. $V_O^{\bullet}$] to $[CaO_{12}]'$. Moreover, the progressive decrease in the PL intensity of ($Ca_{0.99}Nd_{0.01}$)$TiO_3$ powders with the increase of heat treatment temperature is a possible indication that the number of these energy levels within the band gap can be reduced by the increase of structural order into the lattice (Fig. 7a). Therefore, the PL measurements can be a powerful tool in order to investigate a class and/or energy level distribution within the band gap of the materials [104]. Similar spectra to those shown in Fig. 7(a) have been reported in the literature for the $CaTiO_3$ powders [55,105]. Pontes et al. [55] performed experimental and theoretical studies on the PL properties of amorphous $CaTiO_3$ powders obtained by the CPM. According to these authors, the nature of this optical property is associated with the contribution of delocalized electronic levels within the band gap, which are induced by the formation of fivefold Ti–O bonds into this perovskite-type structure. Yang et al. [105] described that the broad PL emissions of $CaTiO_3$ mesocubes are influenced by the structural disorder in the twinned nanodomains.

Broad PL bands were not verified in the ($Ca_{0.99}Nd_{0.01}$)$TiO_3$ powders heat treated from 550 °C to 750 °C (Fig. 7b and c). This behavior is attributed to a reduction of structural defects (oxygen vacancies) or [$TiO_5$. $V_O^{\bullet}$] intermediate complex clusters into the lattice, as consequence of the increase of crystallinity of these powders. Thus, the energy levels responsible for the *p–d* transitions arising from oxygen 2*p* and titanium 3*d* states are drastically reduced within the band gap. Hence, the well-defined narrow bands related to *f–f* transitions of $Nd^{3+}$ ions are predominant in the PL spectra (Fig. 7b and c). The visible luminescence of $Nd^{3+}$ ions corresponding to $4f^{n-1}5d$–$4f^n$ transitions requires appropriate host materials when excited with ultraviolet wavelengths [105–107]. The ground-state of these kinds of ions is characterized by [Xe] $4f^46s^2$ and its PL properties are ascribed to $4f^25d^1$ – $4f^3$ transitions [108]. In this case, during the excitation process of crystalline ($Ca_{0.99}Nd_{0.01}$)$TiO_3$ powders, electron populations can be promoted from ground-state to $^4I_{9/2}$ energy levels. The emission of photons occurs through the decay

**Table 4**
Positions of *f–f* electronic transitions arising from $Nd^{3+}$ ions into the $CaTiO_3$ matrix

| Assignments (*f–f* transitions) | *T* (°C) Symbols | 550 (nm) | 600 (nm) | 650 (nm) | 700 (nm) | 750 (nm) |
|---|---|---|---|---|---|---|
| $^4I_{13/2} \rightarrow {}^4G_{11/2}$ | ★ | 422.1 | 422.1 | 422.6 | 422.6 | 422.6 |
| $^4I_{11/2} \rightarrow {}^4G_{11/2}$ | ○ | 428.1 | 428.1 | 428.6 | 428.6 | 428.6 |
| $^4I_{9/2} \rightarrow {}^4G_{11/2}$ | △ | 435.1 | 435.1 | 435.6 | 435.6 | 435.6 |
| $^4I_{11/2} \rightarrow {}^4K_{15/2}$ | □ | 450.6 | 450.6 | 450.6 | 451.1 | 451.1 |
| $^4I_{11/2} \rightarrow {}^4D_{3/2}$ | ▼ | 454.6 | 454.6 | 454.6 | 455.1 | 455.1 |
| $^4I_{9/2} \rightarrow {}^2K_{15/2}$ | ■ | 458.1 | 458.1 | 458.6 | 458.6 | 458.6 |
| $^4I_{9/2} \rightarrow {}^2D_{3/2}$ | • | 466.1 | 466.1 | 466.6 | 466.1 | 466.1 |
| $^4I_{9/2} \rightarrow {}^2G_{9/2}$ | ♦ | 468.1 | 469.1 | 469.1 | 469.6 | 469.6 |
| $^4I_{9/2} \rightarrow {}^4G_{5/2}$ | ▲ | – | – | – | 585.1 | 585.1 |
| $^4I_{9/2} \rightarrow {}^2G_{7/2}$ | * | – | – | – | 592.1 | 592.1 |
| $^4I_{9/2} \rightarrow {}^4H_{11/2}$ | ♠ | 605.1 | 605.1 | 605.1 | 605.1 | 605.1 |
| $^4I_{9/2} \rightarrow {}^4F_{9/2}$ | ⊕ | 692.1 | 692.1 | 692.1 | 692.1 | 692.1 |
| $^4I_{9/2} \rightarrow {}^2H_{9/2}$ | ▽ | – | – | 800.4 | 800.4 | 800.4 |
| $^4I_{9/2} \rightarrow {}^4F_{5/2}$ | ✠ | – | – | – | 813.1 | 813.1 |

*T* = Temperature and assignments peaks of luminescence for $Nd^{3+}$ ions.

process of electrons situated in $^4I_{9/2}$ energy levels into the empty $^2D_{5/2}$ energy levels [109].

Table 4 shows the corresponding positions to *f–f* electronic transitions arising from $Nd^{3+}$ ions into the $CaTiO_3$ matrix as shown in Fig. 7b and c.

As it can be seen in this table, some electronic transitions shown in the energy level diagram for the $Nd^{3+}$ ions (Fig. 7d) were not observed in the $(Ca_{0.99}Nd_{0.01})TiO_3$ powders because the excitation wavelength (350 nm). In special cases, the literature [110] has reported that the electronic transitions corresponding to $^4I_{9/2}$, $^4I_{11/2}$ and $^4I_{13/2}$ which are in the deep ultraviolet region, could be used to enhance emissions in the visible range. Moreover, the slight shifting verified on the positions referring to *f–f* electronic transitions can be relate to the residual structural defects, effect of the matrix on the local environment of $Nd^{3+}$ ions with its first nearest neighbor anions (oxygen atoms). Can be observed, all *f–f* electronic transitions of $Nd^{3+}$ ions observed in this work are agreement with those reported in the literature [111–115].

## 4. Conclusions

$(Ca_{0.99}Nd_{0.01})TiO_3$ powders were synthesized by the complex polymerization method. XRD patterns, Rietveld refinement and MR spectra confirmed that these powders crystallize in an orthorhombic structure without the presence of deleterious phases. UV–vis spectra indicated that the $E_{gap}$ values of $(Ca_{0.99}Nd_{0.01})TiO_3$ powders are dependent of heat treatment temperature. In fact, high temperatures lead to a decrease of $[TiO_5.\ V_O^Z]$ intermediate complex clusters into the lattice, reducing the presence of intermediary energy levels within the band gap. Consequently, the gradual reduction of these energy levels promotes a progressive increase in the $E_{gap}$ of these materials with perovskite-type structure. Models representing the ordered (symmetric) and disordered (asymmetric) $(Ca_{0.99}Nd_{0.01})TiO_3$ structure were proposed in order to explain the origin of the PL emissions in these ceramic oxides. The PL spectra of the powders exhibited broad and narrow bands when excited with 350 nm wavelengths. The broad PL bands with a maximum emission situated at around 566 nm were observed for the powders heat treated from 300 °C to 500 °C, as consequence of *p–d* transitions arising from oxygen 2*p* and titanium 3*d* states. The increase of heat treatment temperature in the range 550–750 °C promoted a reduction of these energy levels, favoring the predominance of narrow bands in the PL spectra. These narrow bands are arising from typical *f–f* electronic transitions of $Nd^{3+}$ ions.

## Acknowledgements

The authors thank the financial support of the Brazilian research financing institutions: CAPES, CNPq and FAPESP.

## References

[1] X. Liu, R.C. Liebermann, Phys. Chem. Miner. 20 (1993) 171–175.
[2] R.H. Buttner, E.N. Maslen, Acta Crystallogr. B 48 (1992) 644–649.
[3] S.A.T. Redfern, J. Phys. Condens. Matter 8 (1996) 8267–8275.
[4] B.J. Kennedy, C.H. Howard, B.C. Chakoumakos, J. Phys. Condens. Matter 11 (1999) 1479–1488.
[5] D. Talantikite, L. Taïbi-Benziada, Solid State Sci. 11 (2009) 151–155.
[6] B.D. Lee, K.H. Yoon, E.S. Kim, T.H. Kim, Jpn. J. Appl. Phys. 42 (2003) 6158–6161.
[7] T. Fujii, A. Fujishima, T. Hirano, T. Kobayashi, Appl. Phys. Lett. 62 (1993) 3204–3206.
[8] J. Hao, W. Si, X.X. Xi, R. Guo, A.S. Bhalla, L.E. Cross, Appl. Phys. Lett. 76 (2000) 3100–3102.
[9] A. Pashkin, S. Kamba, M. Berta, J. Petzelt, G.D.C.C. de Györgyfalva, H. Zheng, H. Bagshaw, I.M. Reaney, J. Phys. D. Appl. Phys. 38 (2005) 741–748.
[10] E. Motyl, B. Lowkis, E. Rucki, Przeglad Elektrotechniczy 84 (2008) 181–184.
[11] C.L. Huang, J.T. Tsai, Y.B. Chen, Mater. Res. Bull. 36 (2001) 547–556.
[12] K.H. Yoon, W.S. Kim, E.S. Kim, Mater. Sci. Eng. B 99 (2003) 112–115.
[13] M.S. Fu, X.Q. Liu, X.M. Chen, J. Eur. Ceram. Soc. 28 (2008) 585–590.
[14] C.L. Huang, C.H. Shen, T.C. Lin, J. Alloys Compd. 468 (2009) 516–521.
[15] V.V. Lemanov, A.V. Sotnikov, E.P. Sminova, M. Weihnacht, R. Kunze, Solid State Commun. 110 (1999) 611–614.
[16] V.V. Lemanov, A.V. Sotnikov, E.P. Smirnova, M. Weihnacht, Appl. Phys. Lett. 81 (2002) 886–888.
[17] A.V. Stanishevsky, S. Holliday, Surf. Coat. Technol. 202 (2007) 1236–1241.
[18] S. Kaciulis, G. Mattogno, L. Pandolfi, M. Cavalli, G. Gnappi, A. Montenero, Appl. Surf. Sci. 151 (1999) 1–5.
[19] S. Kaciulis, G. Mattogno, A. Napoli, E. Bemporad, F. Ferrari, A. Montenero, G. Gnappi, J. Electron. Spectrosc. Relat. Phenom. 95 (1998) 61–69.
[20] D. Wang, Y. Liu, H. Hu, Z. Zeng, F. Zhou, W. Liu, J. Phys. Chem. C 112 (2008) 16123–16129.
[21] W. Sun, S. Zhang, C. Wang, Z. Liu, Z. Mao, Catal. Lett. 119 (2007) 148–153.
[22] G.Y. Wang, Y.J. Wang, X.W. Zhao, H.T. Zhang, Chin. J. Catal. 26 (2005) 138–142.
[23] H.K. Yang, B.K. Moon, J.H. Jeong, S.S. Yi, P.S. Kim, J.H. Kim, J. Kor. Phys. Soc. 49 (2006) 365–369.
[24] X. Zhang, J. Zhang, X. Ren, X.J. Wang, J. Solid State Chem. 181 (2008) 393–398.
[25] R. Fujiwara, H. Sano, M. Shimizu, M. Kuwabara, J. Lumin. 129 (2009) 231–237.
[26] P.J. Dereń, R. Mahiou, R. Pazik, K. Lemanski, W. Strek, Ph. Boutinaud, J. Lumin. 128 (2008) 797–799.
[27] X. Zhang, J. Zhang, X. Zhang, L. Chen, Y. Luo, X.J. Wang, Chem. Phys. Lett. 434 (2007) 237–240.
[28] A.T. de Figueiredo, S. de Lazaro, E. Longo, E.C. Paris, J.A. Varela, M.R. Joya, P.S. Pizani, Chem. Mater. 18 (2006) 2904–2911.
[29] T. Wanjun, W. Kun, B. Xuhui, C. Donghua, J. Mater. Sci. 42 (2007) 9915–9919.
[30] A.T. de Figueiredo, V.M. Longo, S. de Lazaro, V.R. Mastelaro, F.S. De Vicente, A.C. Hernandes, M.S. Li, J.A. Varela, E. Longo, J. Lumin. 126 (2007) 403–407.
[31] P. Boutinaud, E. Pinel, R. Mahiou, Opt. Mater. 30 (2008) 1033–1038.
[32] K. Goto, Y. Nakachi, K. Ueda, Thin Solid Films 516 (2008) 5885–5889.
[33] G. Branković, V. Vukotić, Z. Branković, J.A. Varela, J. Eur. Ceram. Soc. 27 (2007) 729–732.
[34] V.M. Vukotic, N. Radojevic, L. Zivkovic, Z. Vukovic, B. Stojanovic, Mater. Sci. Forum 494 (2005) 393–398.
[35] G. Mi, Y. Murakami, D. Shindo, F. Saito, Powder Technol. 105 (1999) 162–166.
[36] V. Berbenni, A. Marini, J. Mater. Sci. 39 (2004) 5279–5282.
[37] O.P. Shrivastava, N. Kumar, I.B. Sharma, Bull. Mater. Sci. 27 (2004) 121–126.
[38] A.V. Gorokhovsky, J.I. Escalante-Garcia, T. Sánches-Monjarás, G. Vargas-Gutierrez, Mater. Lett. 58 (2004) 2227–2230.
[39] P. Kar, J.W. Evans, Electroc. Act. 54 (2008) 835–843.
[40] D.T.L. Alexander, C. Schwandt, D.J. Fray, Acta Mater. 54 (2006) 2933–2944.
[41] V.S. Sudavtsova, A.M. Sych, V.G. Kudin, Powder Metall. Metal Ceram. 38 (1999) 466–471.
[42] X. Lu, Z. Guo, S. Luo, T. Lin, S. Yin, J. Yang, J. Chin. Ceram. Soc. 31 (2003) 490–493.
[43] H.C. Yi, J.J. Moore, J. Mater. Sci. 25 (1990) 1159–1168.
[44] Y. Saito, H. Takao, K. Wada, Ceram. Int. 34 (2008) 745–751.
[45] C.H. Jung, D.K. Kim, J. Mater. Synth. Process. 10 (2002) 23–29.
[46] G. Pfaff, Chem. Mater. 6 (1994) 58–62.
[47] M. Manso, M. Langlet, J.M. Martínez-Duart, Mater. Sci. Eng. C 23 (2003) 447–450.
[48] S. Holliday, A. Stanishevsky, Surf. Coat. Technol. 188 (2004) 741–744.
[49] V. Balek, H. Mitamura, T. Banba, M. Bene, Z. Málek, I.N. Beckman, I.M. Bountseva, H. Haneda, T. Mitsuhashi, J. Therm. Anal. Calorim. 80 (2005) 649–654.
[50] V. Ciupina, I. Carazeanu, E. Chirila, G. Prodan, Proc. SPIE 5581 (2004) 345–349.
[51] Q.L. Zhang, H.P. Wang, H. Yang, Chin. J. Inorg. Chem. 22 (2006) 1657–1662.
[52] H. Herrig, R. Hempelmann, Nanostruct. Mater. 9 (1997) 241–244.
[53] B.M. Patil, R.S. Srinivasa, Bull. Mater. Sci. 30 (2007) 225–229.
[54] V.S. Marques, L.S. Cavalcante, J.C. Sczancoski, D.P. Volanti, J.W.M. Espinosa, M.R. Joya, M.R.M.C. Santos, P.S. Pizani, J.A. Varela, E. Longo, Solid State Sci. 10 (2008) 1056–1061.
[55] F.M. Pontes, C.D. Pinheiro, E. Longo, E.R. Leite, S.R. de Lazaro, J.A. Varela, P.S. Pizani, T.M. Boschi, F. Lanciotti, Mater. Chem. Phys. 78 (2003) 227–233.
[56] S. de Lazaro, J. Milanez, A.T. de Figueiredo, V.M. Longo, V.R. Mastelaro, F.S. De Vicente, A.C. Hernandes, J.A. Varela, E. Longo, Appl. Phys. Lett. 90 (2007) 111904–111906.
[57] T.R.N. Kutty, R. Vivekanandan, P. Murugaraj, Mater. Chem. Phys. 19 (1988) 533–546.
[58] D. Wang, Z. Guo, Y. Chen, J. Hao, W. Liu, Inorg. Chem. 46 (2007) 7707–7709.
[59] T.R.N. Kutty, R. Vivekanandan, Mater. Lett. 5 (1987) 79–83.
[60] J.P. Wiff, V.M. Fuenzalida, J.L. Arias, M.S. Fernandez, Mater. Lett. 61 (2007) 2739–2743.
[61] F. Xia, M.V. Raymond, D.M. Smyth, Ferroelectrics 331 (2006) 43–51.
[62] C.C. Chung, Y.L. Chai, Y.S. Chang, J. Phys. Chem. Solids 69 (2008) 1877–1882.
[63] T. Bak, J. Nowotny, P.J. Blennerhassett, Adv. Appl. Ceram. 106 (2007) 101–104.
[64] S.K. Manik, S.K. Pradhan, M. Pal, Physica E 25 (2005) 421–424.
[65] I.L.V. Rosa, A.P.A. Marques, M.T.S. Tanaka, D.M.A. Melo, E.R. Leite, E. Longo, J.A. Varela, J. Fluoresc. 18 (2008) 239–245.
[66] L.S. Cavalcante, V.S. Marques, J.C. Sczancoski, M.T. Escote, M.R. Joya, J.A. Varela, M.R.M.C. Santos, P.S. Pizani, E. Longo, Chem. Eng. J. 143 (2008) 299–307.
[67] http://icsdweb.fiz-karlsruhe.de/.
[68] T.J.B. Holland, S.A.T. Redfern, Miner. Mag. 61 (1997) 65–77.
[69] H.M. Rietveld, J. Appl. Crystallogr. 2 (1969) 65–71.
[70] A.C. Larson, R.B. Von Dreele, Los Alamos National Laboratory Report No. LAUR (2004) p. 86.
[71] L.W. Finger, D.E. Cox, A.P. Jephcoat, J. Appl. Crystallogr. 27 (1994) 892–900.
[72] P.W. Stephens, J. Appl. Crystallogr. 32 (1999) 281–289.

[73] Z. Zhang, G.R. Lumpkin, C.J. Howard, K.S. Knight, K.R. Whittle, K. Osaka, J. Solid State Chem. 180 (2007) 1083–1092.
[74] S.K. Manik, S.K. Pradhan, Mater. Chem. Phys. 86 (2004) 284–292.
[75] M.S. Fu, X.Q. Liu, X.M. Chen, J. Eur. Ceram. Soc. 28 (2008) 585–590.
[76] S. Tripathi, D. Pandey, S.K. Mishra, P.S.R. Krishna, Phys. Rev. B 77 (2008) 052104–052107.
[77] O.P. Shrivastava, N. Kumar, I.B. Sharma, Mater. Res. Bull. 40 (2005) 731–741.
[78] I.R. Evans, J.A.K. Howard, T. Sreckovic, M.M. Ristic, Mater. Res. Bull. 38 (2003) 1203–1213.
[79] R. Ali, M. Yashima, J. Solid State Chem. 178 (2005) 2867–2872.
[80] Y. Li, S. Qin, F. Seifert, J. Solid State Chem. 180 (2007) 824–833.
[81] I. Levin, E. Cockayne, M.W. Lufaso, J.C. Woicik, J.E. Maslar, Chem. Mater. 18 (2006) 854–860.
[82] H. Zheng, I.M. Reaney, G.D.C.C. de Gyorgyfalva, R. Ubic, J. Yarwood, M.P. Seabra, V.M. Ferreira, J. Mater. Res. 19 (2004) 488–495.
[83] H. Zheng, G.D.C.C. de Gyorgyfalva, R. Quimby, H. Bagshaw, R. Ubic, I.M. Reaney, J. Yarwood, J. Eur. Ceram. Soc. 23 (2003) 2653–2659.
[84] T. Hirata, K. Ishioka, M. Kitajima, J. Solid State Chem. 124 (1996) 353–359.
[85] U. Balachandran, N.G. Eror, Solid State Commun. 44 (1982) 815–818.
[86] S. Qin, X. Wu, F. Seifert, A.I. Becerro, J. Chem. Soc. Dalton Trans. 19 (2002) 3751–3755.
[87] D.L. Wood, J. Tauc, Phys. Rev. B 5 (1972) 3144–3152.
[88] A.H. Kahn, A.J. Leyendecker, Phys. Rev. 135 (1964) A1321–A1325.
[89] Y. Pan, Q. Su, H. Xu, T. Chen, W. Ge, C. Yang, M. Wu, J. Solid State Chem. 174 (2003) 69–73.
[90] H.W. Eng, P.W. Barnes, B.M. Auer, P.M. Woodward, J. Solid State Chem. 175 (2003) 94–109.
[91] H. Mizoguchi, K. Ueda, M. Orita, S.C. Moon, K. Kajihara, M. Hirano, H. Hosono, Mater. Res. Bull. 37 (2002) 2401–2406.
[92] L. Grabner, S.E. Stokowski, Phys. Rev. B 2 (1970) 4351–4353.
[93] http://www.crystalimpact.com/diamond.
[94] M. Yashima, R. Ali, Solid State Ionics 180 (2009) 120–126.
[95] M.A. Gomez, M.A. Griffin, S. Jindal, K.D. Rule, V.R. Cooper, J. Chem. Phys. 123 (2005) 094703–094712.
[96] J. Zeng, Y. Li, D. Wang, Q. Yin, Solid State Commun. 133 (2005) 553–557.
[97] H. Samata, D. Kimura, S. Mizusaki, Y. Nagata, T.C. Ozawa, A. Sato, J. Alloys Compd. 468 (2009) 566–570.
[98] N.M. Novikovskii, E.S. Nazarenko, A.A. Novakovich, R.V. Vedrinskii, Bull. Russ. Acad. Sci. Phys. 72 (2008) 431–433.
[99] Y. Hanajiri, T. Matsui, Y. Arita, T. Nagasaki, H. Shigematsu, T. Harami, Solid State Ionics 108 (1998) 343–348.
[100] E.R. Vance, R.A. Day, Z. Zhang, B.D. Begg, C.J. Ball, M.G. Blackford, J. Solid State Chem. 124 (1996) 77–82.
[101] V.M. Longo, A.T. de Figueiredo, S. de Lazaro, M.F. Gurgel, M.G.S. Costa, C.O. Paiva-Santos, J.A. Varela, E. Longo, V.R. Mastelaro, F.S. De Vicente, A.C. Hernandes, R.W.A. Franco, J. Appl. Phys. 104 (2008) 023515–023526.
[102] L.S. Cavalcante, M.F.C. Gurgel, E.C. Paris, A.Z. Simões, M.R. Joya, J.A. Varela, P.S. Pizani, E. Longo, Acta Mater. 55 (2007) 6416–6426.
[103] F.A. Kröger, H.J. Vink, F. Seitz, D. Turnbull, Solid State Physics, third ed., Academic Press, New York, 1956, p. 307.
[104] F. Montoncello, M.C. Carotta, B. Cavicchi, M. Ferroni, A. Giberti, V. Guidi, C. Malagu, G. Martinelli, F. Meinardi, J. Appl. Phys. 94 (2003) 1501–1505.
[105] X. Yang, I.D. Williams, J. Chen, J. Wang, H. Xu, H. Konishi, Y. Pan, C. Liang, M. Wu, J. Mater. Chem. 18 (2008) 3543–3546.
[106] R. Bazzi, A. Brenier, P. Perriat, O. Tillement, J. Lumin. 113 (2005) 161.
[107] I.G. Rubio, J.A. Pardo, R.I. Merino, R. Cases, V.M. Orera, J. Lumin. 86 (2000) 147–153.
[108] M.L. Feng, J.G. Mao, J. Alloys Compd. 388 (2005) 23–27.
[109] M.C. Silva, A.S.S. de Camargo, L.A.O. Nunes, R.A. Silva, A. Marletta, J. Non-Cryst. Solids 354 (2008) 5496–5503.
[110] M. Qureshi, H.Y. Chen, C.H. Lu, Solid State Commun. 142 (2007) 85–88.
[111] F.H. Cristovan, C.M. Nascimento, M.J.V. Bell, E. Laureto, J.L. Duarte, I.F.L. Dias, W.O. Cruz, A. Marletta, Chem. Phys. 326 (2006) 514–520.
[112] M.C. Silva, F.H. Cristovan, C.M. Nascimento, M.J.V. Bell, W.O. Cruz, A. Marletta, J. Non-Cryst. Solids 352 (2006) 5296–5300.
[113] Y.C. Ratnakarama, N.V. Srihari, A.V. Kumar, D.T. Naidu, R.P.S. Chakradhar, Spectrochim. Acta A 72 (2009) 171–177.
[114] K. Kumar, S.B. Rai, A. Rai, Spectrochim. Acta A 71 (2008) 508–512.
[115] F.H. Cristovan, S.P. Eiras, W.O. Cruz, A. Marletta, D.T. Balogh, E. Laureto, J.L. Duarte, I.F.L. Dias, Quimica Nova 28 (2005) 964–967.